# PERFORMANCE OF $NB_3SN$ QUADRUPOLE MAGNETS UNDER LOCALIZED THERMAL LOAD

V. V. Kashikhin, R. Bossert, G. Chlachidze, M. Lamm, N. V. Mokhov, I. Novitski, A.V. Zlobin

Fermi National Accelerator Laboratory
Batavia, IL, 60510, USA

## ABSTRACT

This paper describes the results of design and analyses performed on 120-mm $Nb_3Sn$ and NbTi quadrupole magnets with parameters relevant for the LHC IR upgrade. A realistic radiation heat load is evaluated in a wide luminosity range and translated into the magnet quench performance. The simulation results are supported by thermal measurements on a 90-mm $Nb_3Sn$ quadrupole coil.

**KEYWORDS:** Superconducting magnets, quench margin, thermal analysis, radiation.

## INTRODUCTION

$Nb_3Sn$ accelerator magnet technology for particle accelerators is being extensively developed around the world. Due to the high critical temperature, $Nb_3Sn$ magnets may be an attractive option for high-luminosity interaction regions of hadron colliders, where the accelerator components are exposed to strong radiation showers from the interaction point.

One of the possible applications for the $Nb_3Sn$ technology is the IR quadrupole magnets for the LHC Phase II upgrade to the luminosity of $10^{35}$ $cm^{-2}s^{-1}$. Conceptual design of the Phase I LHC IR upgrade has stipulated the preferred NbTi quadrupole coil aperture of 120 mm and the operating gradient of ~120 T/m for the 10 m long magnet [1]. The coil prestress is delivered by means of the self-supporting stainless steel (SS) collars. It mechanically decouples the coil from the iron yoke and allows four 110-mm holes in the yoke for the internal heat exchangers, which is perceived as the preferred solution.

The US LHC Accelerator Research Program (LARP) is working on the development of a 120-mm $Nb_3Sn$ quadrupole magnet (HQ) [2] that can be a candidate for the Phase II upgrade with the same beam optics. The structural concept of the HQ magnet is based on the bladder-and-shell approach that relies on the iron yoke as an important structural element in creating the coil prestress. By that reason, it may be challenging to accommodate the large iron yoke holes of the Phase I design without compromising the HQ support structure.

An alternative design approach to the Phase II upgrade is analyzed in this report. It is based on the idea of replacing the NbTi coils with those made of $Nb_3Sn$ inside the mechanical structure identical to the one of the Phase I upgrade. In addition to the ability of re-utilizing most of the infrastructure and tooling used for the Phase I magnets, it would also require minimal modifications to the cryogenic system, leading to substantial cost and time savings. That approach was evaluated in terms of the magnetic and thermal designs.

Thermal performance of IR magnets is strongly dependent on the characteristics of superconductor, type, and size of the coil insulation, as well as the cooling scheme. In this respect, it is important to study the magnet characteristics under the relevant thermal loads, both numerically and experimentally.

One of the LARP technological quadrupole models (TQC02b) was equipped with a special strip heater to perform the experimental studies of operating margin in a $Nb_3Sn$ quadrupole [3]. The SS heater was placed in the inner layer (IL) midplane, where the radiation-induced heat depositions exhibit the maximum, between the adjacent coils made of MJR strand. The test yielded good agreement with the simulations and provided important information for tuning the numerical model.

It is known that because cooling conditions for the coil outer layer (OL) are generally worse than that for the IL, the peak temperature in the OL under the realistic heat dissipations may exceed that of the IL [4]. In addition, the most likely candidate for use in future $Nb_3Sn$ magnets is the high-Jc RRP conductor. For these reasons, one of the TQ coils based on the RRP conductor was equipped with dedicated strip heaters for both inner and OLs. It permitted independent adjustment of the thermal load in each layer in order to reproduce more realistic heat distribution due to the beam operations.

## 120-MM QUADRUPOLE MAGNET

### Magnetic Design

Magnetic design and optimization of the 120-mm IR quadrupole magnet was performed by ROXIE code with non-linear properties of the yoke steel. TABLE 1 lists the cable parameters used in the coil design. The cable width was set close to the width of the LHC main dipole cable that is considered for the Phase I magnets. The strand diameter was, however, fixed at 0.7 mm that allowed to reach 80-90% of the short sample limit in most of the LARP TQ magnets based on the high-$J_c$ RRP strands [5]-[6]. For comparison purposes, a design based on NbTi cable with the same dimensions was also analyzed.

FIGURE 1 shows the coil and iron yoke cross-section with the flux density plot in the yoke and TABLE 1 presents the main magnet parameters for the two types of superconductor. The $Nb_3Sn$ coil length is limited to ~6m by the size of the available (at FNAL) reaction oven. The 10 m long magnet would have to be made out of two coils stacked together inside of the common cold mass. That would invariably introduce a longitudinal gap between the coils and lead to reduction of the integrated field strength.

To compensate that reduction, the operating gradient of the $Nb_3Sn$ design was set at 130 T/m. The largest of the geometrical harmonics, minimized at that gradient, was $b_{18}$=-0.42 units, at the reference radius of 40 mm. The superconductor properties were parameterized according to [7]-[8] with the reference parameters listed in TABLE 1.

The $Nb_3Sn$ magnet has an ample operating margin at either temperature, while the NbTi version requires 1.9 K operation. The quench gradient at that temperature for the NbTi cable is slightly lower than 149 T/m quoted in [1]. That difference is due to the smaller cable thickness and lower compaction factor driven by the $Nb_3Sn$ strand, resulting in lower engineering current density in the coil with respect to the case based on the LHC dipole cable. Note that the values posted in the table do not account for the coil heating due to the radiation that is subject of a separate paragraph.

**TABLE 1**. Parameters of the 120-mm quadrupole magnets based on $Nb_3Sn$ and NbTi strands

| Parameter | Unit | $Nb_3Sn$ | NbTi |
|---|---|---|---|
| Number of strands | - | 40 | |
| Strand diameter | mm | 0.700 | |
| Cable inner thickness bare) | mm | 1.171 | |
| Cable outer thickness (bare) | mm | 1.344 | |
| Cable width (bare) | mm | 15.15 | |
| Reference field $B_{ref}$ | T | 12 | 5 |
| Reference non-Cu $J_c$ at $B_{ref}$, 4.2 K | $A/mm^2$ | 2500 | 3000 |
| Copper to non-copper ratio | - | 0.87 | 1.3 |
| Insulation material | - | S-2 glass | Kapton |
| Insulation thickness | mm | 0.100 | |
| Aperture diameter, mm | mm | 120 | |
| Yoke outer diameter, mm | mm | 275 | |
| Number of turns/aperture | | 200 | |
| *Quench parameters* | | | |
| Quench gradient at 4.5K | T/m | 188.8 | 106.7 |
| Quench current at 4.5K | kA | 15.21 | 8.38 |
| Quench peak field at 4.5K | T | 13.07 | 7.38 |
| Quench gradient at 1.9K | T/m | 207.0 | 143.8 |
| Quench current at 1.9K | kA | 16.74 | 11.44 |
| Quench peak field at 1.9K | T | 14.32 | 9.95 |
| *Operating parameters* | | | |
| Operating gradient | T/m | 130 | 120 |
| Operating current | kA | 10.30 | 9.47 |
| Operating peak field | T | 9.00 | 8.30 |
| Operating inductance | mH/m | 9.22 | 9.26 |
| Operating stored energy | kJ/m | 489.1 | 415.3 |

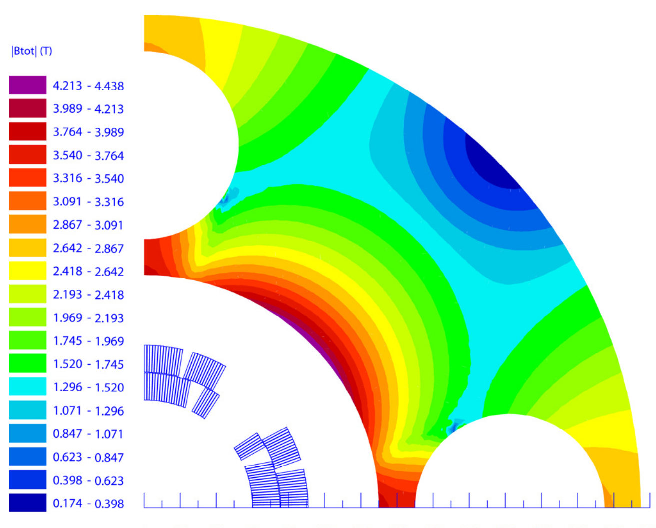


**FIGURE 1.** Cross-section of the 120-mm quadrupole magnet.

## Radiation Analysis

The LHC IP5 optics layout based on $Nb_3Sn$ quadrupoles, as described in [9], was adjusted for the Phase II parameters and implemented in the MARS15 model of that region [10]-[11]. FIGURE 2 shows the longitudinal structure of the final focus region with the particle tracks from the interaction point. In addition to the magnet features described above, the model included beam pipe, cold bore, and cooling channels. As proposed in [12], 3-mm SS segment absorbers were also implemented in the model.

The principal results of the MARS15 simulations on the power density in the $Nb_3Sn$ coil are shown in FIGURE 3. The peak power deposition averaged in the midplane cable of IL at the non-IP end of the Q1 is 2.4 mW/g with the SS absorbers.

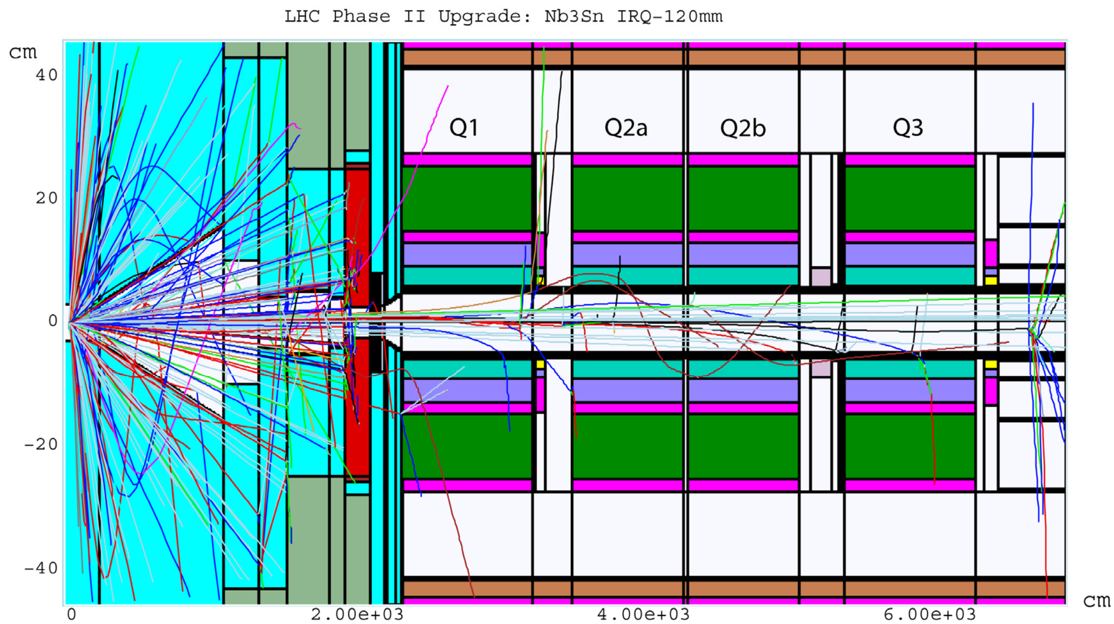


**FIGURE 2. Schematic view of the IP5 MARS15 model with particle tracks from the IP shown.**

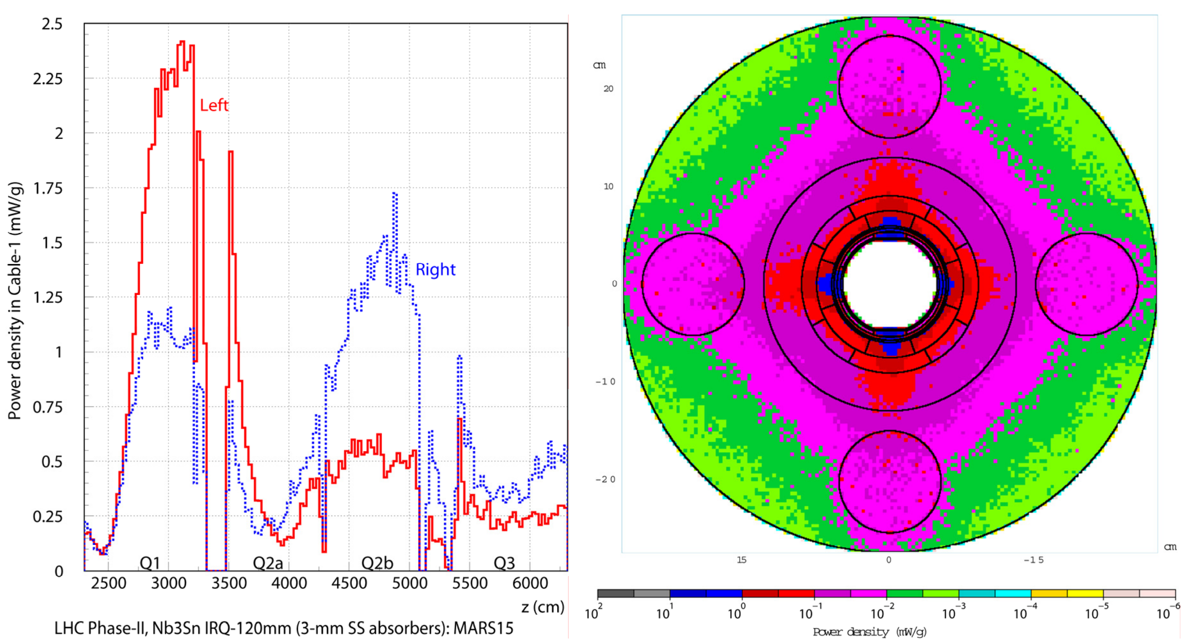


**FIGURE 3. Longitudinal distribution of the peak power density in the coil (left) and power density isocontours in Q1 at the longitudinal peak (right).**

**Thermal Analysis**

The MARS simulation produced a heat load map in all magnet elements for the luminosity of $10^{35}$ $cm^{-2}s^{-1}$. A transverse cross-section of that map at the longitudinal maximum (non-IP end of Q1) was imported into the thermal model within COMSOL Multiphysics code. It was linearly scaled to explore a wide range of operating luminosities.

The thermal model included all the features of the $Nb_3Sn$ coil. It had the following types of insulation impregnated with epoxy: 0.100-mm of S-2 glass around the cables, wedges, and poles; 0.127-mm of S-2 glass at the inner and outer coil surfaces; 0.254-mm of S-2 glass between the layers. The ground insulation was 0.254-mm of Kapton.

Temperature dependencies of thermal properties were also taken into account for all materials. The thermal conductivities of copper, bronze, SS, low carbon steel, and insulation were parameterized by analytical functions [13]-[14]. The thermal properties of epoxy-impregnated S-2 glass insulation were approximated by the properties of a fiberglass composite (G10). In case of NbTi coil, the G10 properties were replaced with those of Kapton. The analysis was performed for the collars made of SS and aluminum (Al).

The boundary conditions included the fixed helium bath temperature $T_0$ at the inner coil surface, outer yoke surface, and the heat exchanger surface, which are in direct contact with liquid helium. It was assumed that the $Nb_3Sn$ coil impregnation and NbTi coil curing prevents helium penetration inside of the coil and all heat is extracted through the insulation. The Kapitza resistance measured on epoxy-impregnated fiberglass tapes [15] is ~4.4 $cm^2KW^{-1}$ at $T_0$ = 1.9 K, while the effective thermal resistance of the insulation between bare cable and superfluid helium is at least an order of magnitude larger. Because of that, the Kapitza resistance was neglected. It was also assumed that the thermal contact resistances between different materials are negligibly small. The heat flux to normal liquid helium was monitored and compared with the critical value. No cooling channels in the collars were considered, except as noted below.

FIGURE 4 shows the calculated quench gradients as functions of the luminosity for the $Nb_3Sn$ and NbTi magnets. The average power density in the midplane cable of the IL is also quoted in the plots. All curves for the $Nb_3Sn$ magnet exhibit the same shape with two knees. At the low power depositions, the magnet quenches are in the pole turn of the IL with practically no difference between Al and SS collars. Starting at the luminosity of ~$4x10^{35}$ $cm^{-2}s^{-1}$, the quenches move to the midplane turn of the IL yielding the first knee. It is where the advantage of the Al collar becomes visible. At the very large heat depositions, the quench point shifts to the midplane turn of the OL, corresponding to the second knee.

The luminosity data much higher than that of the Phase II upgrade have purely academic interest, unless there is a need to reduce the liner thickness. However, as shown below, the cross-calibration with the heater tests falls into that region. The reduction of quench gradient at the nominal luminosity of the Phase II upgrade is ~1% for the $Nb_3Sn$ magnet that allows it to operate at 60-70% of the short sample limit, depending on the $T_0$.

The thermal performance changes dramatically for the NbTi magnet due to the lower critical temperature of NbTi and worse thermal properties of Kapton insulation. The shape of the quench curve for the SS collars is essentially the same as in the $Nb_3Sn$ case. Changing the collar material to Al gives a visible improvement in the quench performance of 2.5% at the nominal luminosity of Phase I upgrade.

As a reference, a fully transparent collar was modeled by applying the boundary condition of $T_0$ at the outer coil surface. It shows a minor advantage with respect to the Al collars in terms of the quench performance. In addition, the reductions of quench gradient at the nominal luminosity of the Phase I upgrade are relatively small – around 3% in the cases of Al or fully transparent collars even without helium penetration inside of the coil.

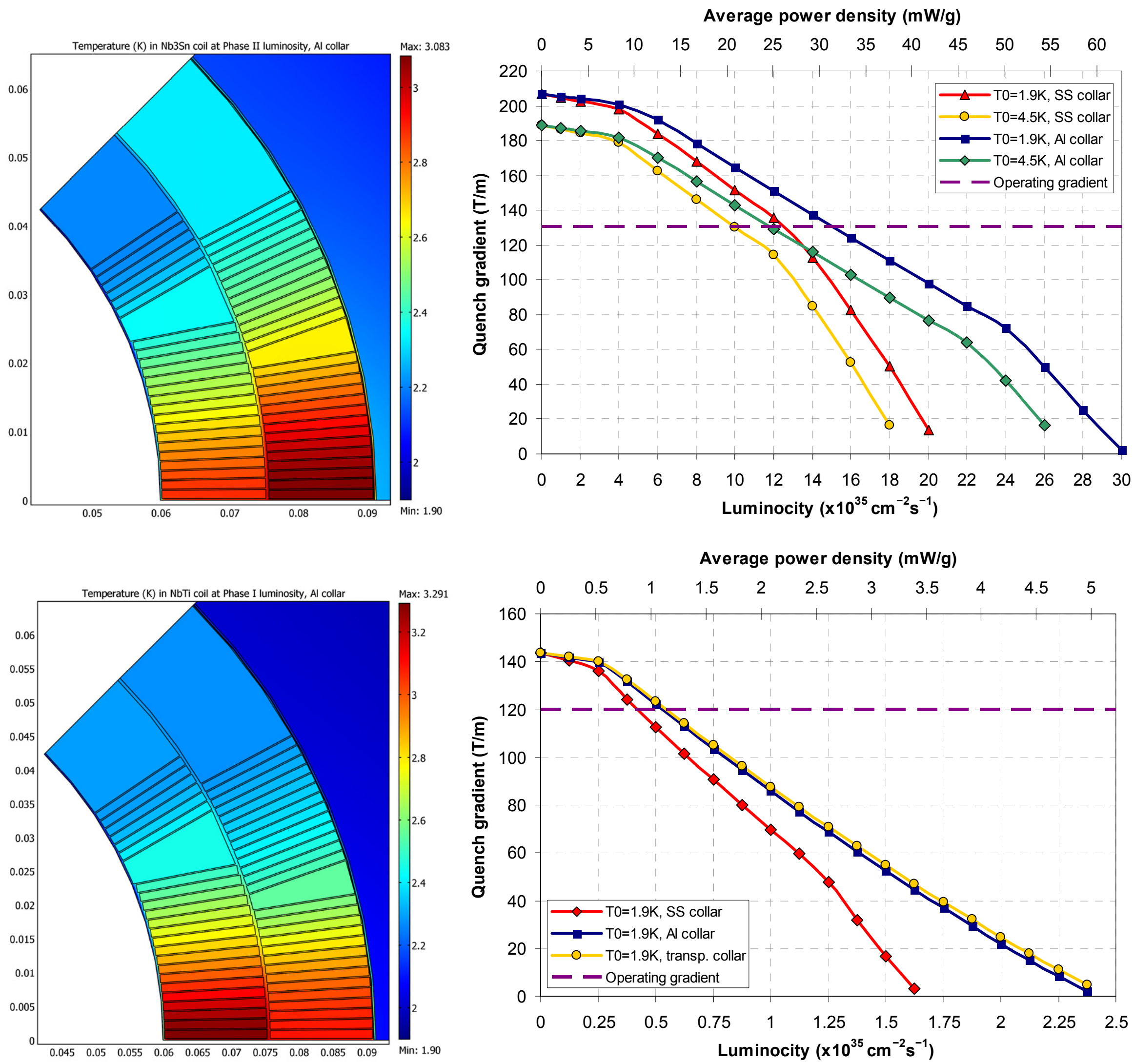


**FIGURE 4. Coil temperature distributions at projected luminosities (left) and quench gradients as functions of the luminosity (right) in $Nb_3Sn$ (top) and NbTi (bottom) magnets.**

## 90-MM TQM MODEL

In order to perform independent TQ coil tests, a magnetic mirror structure was designed and built at Fermilab. Details of the magnetic and mechanical designs and quench performance are summarized in [16]. One of the mirror models – TQM02 was equipped with the strip heaters to evaluate the RRP coil performance under the localized heat load. Four SS heaters were placed next to the midplane turns of both layers and octants. The heaters could be powered alone or together using separate power supplies.

### Thermal analysis

The thermal analysis of TQM model was performed using COMSOL Multiphysics code. Details of the coil insulation are given in [16]. The assumptions on the material properties were the same as for the 120-mm quadrupole above. The boundary conditions included a constant temperature $T_0$ on all surfaces that are in contact with liquid helium. FIGURE 5 presents the temperature distribution in the coil for different heater operations.

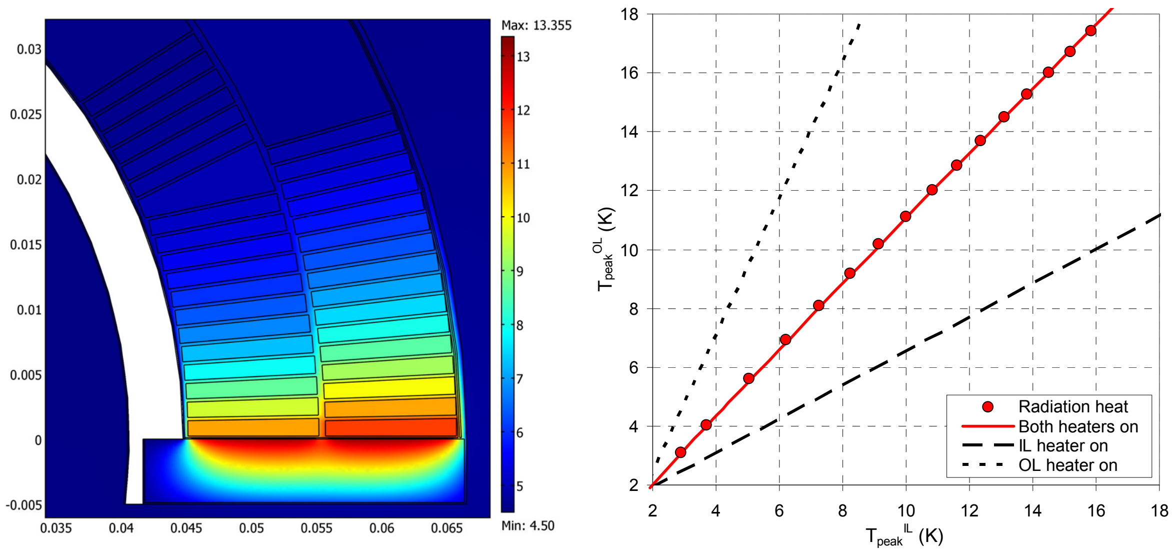


**FIGURE 5. Temperature distribution in the coil with both heaters on (left, $P^{IL}$ = 10 W/m, $P^{OL}$ = 7.5 W/m) and OL peak temperature as function of the IL temperature (right).**

When the heaters are individually powered, the maximum coil temperature is in the cable adjacent to the heater. The temperature dependence corresponding to the realistic radiation heat in the 120-mm $Nb_3Sn$ magnet design with Al collars is also shown in the plot. It falls in between the lines of independent heater operations, making it possible to reproduce the realistic temperature profile in the midplane turns using both heaters.

It was found that when the OL heater operates at 75% of the IL heater power, the temperature distribution in the midplane turns is nearly identical to that of the 120-mm magnet under the radiation heat depositions. That power ratio was maintained during the heater tests by two power supplies. Because of the localized nature of the heat source, the temperature gradient in the azimuthal direction is higher than that due to the radiation heat depositions, practically excluding influence of the pole turns on the thermal performance.

## Measurements

TQM02 magnet was tested at 1.9 K and 4.5 K temperatures at Fermilab's Vertical Magnet Test Facility. The heater tests were performed after the magnet was trained. FIGURES 6-7 show the quench currents during the individual and simultaneous heater tests. During the individual heater tests, the power was delivered to a single heater of either transition (T) side or non-transition (NT) side of either inner or OL. During the simultaneous heater tests, the power was delivered to both inner and OL heaters of the same side in the 1/0.75 proportion defined above.

Because of the non-symmetric magnet geometry with respect to the coil midplanes and a thick thermal insulator (G10) between heaters and the mirror block, a larger than ½ fraction of the total heat flux was flowing into the coil. Due to the non-linear material properties, that fraction varied within 76%-80%, depending on the regime. However, the heat flux distribution between IL and OL during the simultaneous heater tests was practically constant and equal to 1/0.69. The change in the heat flux distribution with respect to the power distribution is due to the non-symmetric placement of the G10 spacer with respect to the center of the coil midplane, as shown in the plot above. The 1.9 K measurements were primarily done for the NT coil side that had better correlation of quench location with the heater position than the other side.

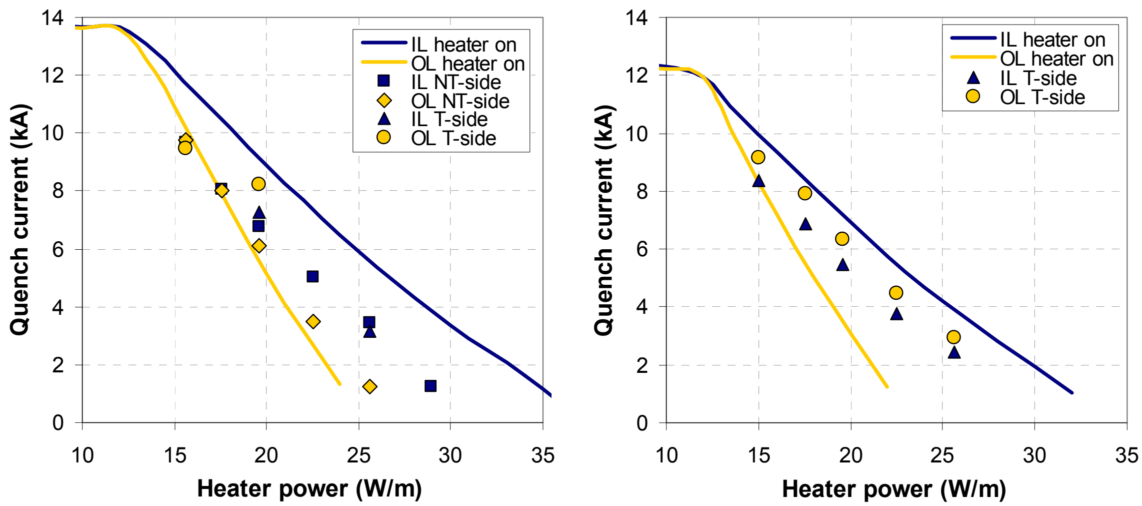


**FIGURE 6. Quench current as function of the heater power during individual heater tests at $T_0$=1.9 K (left) and $T_0$=4.5 K (right). Solid lines represent calculations and markers represent measurements.**

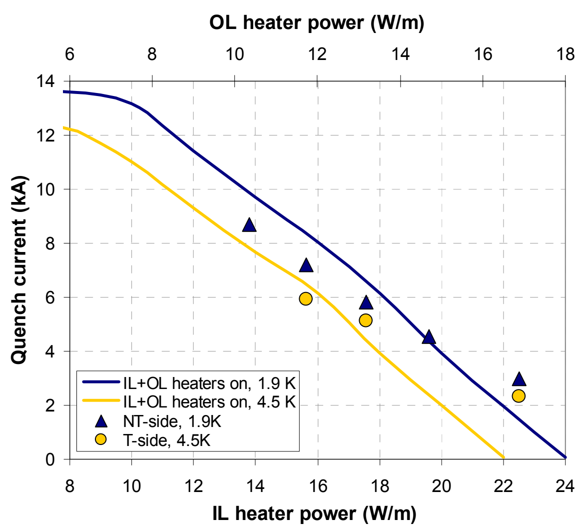


**FIGURE 7. Quench current as function of the heater power during both heater tests. Solid lines represent calculations and markers represent measurements.**

The coil performed consistently worse than expected during the IL heater tests, while the OL performance was very close to the expectations. A possible cause of that difference could be hindered cooling of the IL due to the epoxy buildup at the inner coil surface [16].

During the 4.5 K tests, all quenches triggered by the NT heaters were in the leads that forced studies on the T side. The IL performance was similar to that of the 1.9 K tests. However, the OL demonstrated unexpectedly large quench currents, exceeding those of the IL. The reason of such behavior needs to be understood.

The magnet performance during the simultaneous heater tests was consistent with the individual heater measurements. In the medium power region (10-18 W/m), the quenches were determined by the IL midplane, demonstrating ~10 % reduction with respect to the calculated values. In the high power region, the quenches moved to the OL, where the magnet performed better than expected, especially at 4.5 K.

## SUMMARY

A 120-mm $Nb_3Sn$ quadrupole magnet compatible with the cryogenic system of the LHC Phase I upgrade was analyzed in terms of the magnetic, radiation and thermal performances. That magnet can operate at 60-70% of the short sample limit under the heat load corresponding to the luminosity of the Phase II upgrade at either 1.9 K or 4.5 K. It has a potential for the heat load raise by a factor of four beyond the level of Phase II upgrade with only a minor reduction in the operating margin, provided the cryogenic system is capable of extracting the heat from the cryostat without film boiling at the cooling surfaces.

The thermal simulations indicate that a reference NbTi magnet based on the same 120-mm coil cross-section can withstand the heat load of the Phase I upgrade with a minor reduction in the quench margin. Reaching higher luminosities with NbTi magnet is, however, problematic unless an efficient heat extraction from the coil is realized.

In order to reproduce the realistic heat loads, one of the 90-mm $Nb_3Sn$ models was equipped with midplane strip heaters. The measurements demonstrated a maximum reduction of the quench currents by 10 % with respect to the calculated values that can be treated as an uncertainty encompassing possible variations of the insulation thicknesses and thermal conditions in a real coil. It should not be an issue, given the ample thermal margin of the $Nb_3Sn$ magnet at the Phase II luminosity.

## REFERENCES


1. V. Baglin et al., "Conceptual Design of the LHC Interaction Region Upgrade – Phase-I", LHC Project Report 1163.
2. H. Felice, et al., "Design of HQ – a High Field Large Bore $Nb_3Sn$ Quadrupole Magnet for LARP", *IEEE Trans. Appl. Supercond.*, to be published in June 2009.
3. V. V. Kashikhin, et al., "Quench Margin Measurement in $Nb_3Sn$ Quadrupole Magnet", *IEEE Trans. Appl. Supercond.*, to be published in June 2009.
4. I. Novitski and A. V. Zlobin, "Thermal Analysis of SC Quadrupoles in Accelerator Interaction Regions," *IEEE Trans. Appl. Supercond.*, vol. 17, no. 2, Jun. 2007, pp. 1059-1062.
5. R.C. Bossert, et al., "Fabrication and Test of LARP Technological Quadrupole Models of TQC Series", *IEEE Trans. Appl. Supercond.*, to be published in June 2009.
6. S. Caspi, et al., "Test Results of LARP Nb3Sn Quadrupole Magnets Using a Shell-based Support Structure (TQS)", *IEEE Trans. Appl. Supercond.*, to be published in June 2009.
7. L. T. Summers, et al., "A model for the prediction of $Nb_3Sn$ critical current as a function of field, temperature, strain, and radiation damage," *IEEE Trans. Magn.*, vol. 27, no. 2, 1991, pp. 2041-2044.
8. A. Devred, CEA/Saclay, *Review of Superconducting Dipole and Quadrupole Magnets for Particle Accelerators*, DAPNIA/STCM 98-07, August 1998.
9. J.A. Johnstone, et al., "Optics Implications of Implementing $Nb_3Sn$ Magnets In the LHC Phase I Upgrade", *Proc. 2008 European Particle Accel. Conf.,* pp. 2626-2628.
10. N.V. Mokhov, http://www-ap.fnal.gov/MARS/.
11. N.M. Mokhov, et al., Fermilab-FN-732 (2003), LHC Project Report 633.
12. N.V. Mokhov, I.L. Rakhno, "Mitigating Radiation Loads in $Nb_3Sn$ Quadrupoles for the CERN LHC Upgrades", *Phys. Rev. STAB* **9**, 101001 (2006).
13. E. D. Marquardt, J. P. Le and R. Radebaugh, "Cryogenic Material Properties Database," in *Proc. 11th Int. Cryocooler Conf.,* Jun. 2000, Keystone, Colorado.
14. J. E. Jensen, et al., *Brookhaven National Laboratory Selected Cryogenic Data Notebook*, BNL 10200-R, vol. I, 1980.
15. B. Baudouy and J. Polinski, "Thermal conductivity and Kapitza resistance of epoxy resin fiberglass tape at superfluid helium temperature", *Cryogenics* **49**, pp. 138–143 (2009).
16. A. V. Zlobin et al., "Testing of $Nb_3Sn$ quadrupole coils using magnetic mirror structure", presented at CEC/ICMC 2009.